Hairy Hybrid Nanoparticles of Magnetic Core, Fluorescent Silica Shell, and Functional Polymer Brushes

ARTICLE *in* MACROMOLECULES · NOVEMBER 2009

Impact Factor: 5.8 · DOI: 10.1021/Ma901592j

6 AUTHORS, INCLUDING:

Guoliang Li
Chinese Academy of Sciences
26 PUBLICATIONS **1,016** CITATIONS
SEE PROFILE

Liang Wang
83 PUBLICATIONS **749** CITATIONS
SEE PROFILE

B. Y. Zong
National University of Singapore
58 PUBLICATIONS **605** CITATIONS
SEE PROFILE

Macromolecules
NOTE

Macromolecules **2009**, *42*, 8561–8565 **8561**
DOI: 10.1021/ma901592j

Hairy Hybrid Nanoparticles of Magnetic Core, Fluorescent Silica Shell, and Functional Polymer Brushes

Guoliang Li, Dawn Liming Zeng, Liang Wang, Baoyu Zong, K. G. Neoh, and E. T. Kang*

Department of Chemical & Biomolecular Engineering, National University of Singapore, Kent Ridge, Singapore 119260

Received July 21, 2009; Revised Manuscript Received September 4, 2009

1. Introduction

Superparamagnetic nanoparticles of iron oxides have been of great interest because of their potential applications in cell targeting, drug delivery, bioseparation, and magnetic resonance imaging (MRI).[1−5] Recently, numerous methods have been developed to synthesize magnetic and fluorescent composite particles with core−shell structures to broaden the applications of these nanoparticles in biosensors and diagnostic medical devices.[6−8] For these applications, the nanoparticles should have improved biocompatibility to evade the immune system. Nanoparticles with poor dispersity will agglomerate after being assimilated into living systems. Therefore, it is highly desirable to further tailor the surface functionality of these magnetic and fluorescent nanoparticles, for example, via grafting of hydrophilic and biocompatible components.

Interdisciplinary approaches involving inorganic and polymer syntheses have provided new opportunities for designing and fabricating novel inorganic/organic hybrid nanostructures.[9,10] Some polymeric materials of novel structures and functionality have also been developed via combined chemical synthesis routes.[11−14] For instance, multicomponent stimuli-responsive ultrathin polymer films have been prepared via combined layer-by-layer (LbL) assembly and atom transfer radical polymerization (ATRP).[11] Cylindrical core−shell brushes have been prepared by a combination of ring-opening polymerization (ROP) and ATRP.[12] Reversible addition−fragmentation chain transfer (RAFT) polymerization and click chemistry have been combined to produce well-defined block copolymers,[13] comblike copolymers,[14] and stimuli-responsive polymer−protein bioconjugates.[15] Thus, combination of different polymerization methods to produce unique structures and properties holds great promise.[16] Distillation−precipitation polymerization (DPP) is another novel technique for synthesizing micro- and nanospheres with core−shell or hollow structures.[17−19] On the other hand, ATRP, as a "controlled" radical polymerization method, allows the synthesis of well-defined and narrowly distributed polymer brushes with "living" chain ends on various types of substrates.[20−24] In this work, we report a combined approach of inorganic sol−gel reaction, DPP and ATRP, to produce multifunctional hybrid nanoparticles of iron oxide (Fe_3O_4) core, fluorescent dye-sensitized silica shell ($DySiO_2$), and well-defined poly(poly(ethylene glycol) methacrylate) (P(PEGMA)) biocompatible brushes.

2. Results and Discussion

Procedures for the syntheses of magnetic and fluorescent $Fe_3O_4/DySiO_2$ and $Fe_3O_4/DySiO_2$-*g*-P(PEGMA) hybrid nanoparticles are illustrated in Scheme 1.

*To whom correspondence should be addressed. E-mail: cheket@nus.edu.sg.

Scheme 1. Synthesis of the Hairy Hybrid Nanoparticles with a Magnetic Core, Fluorescent Silica Shell, and Functional Polymer Brushes

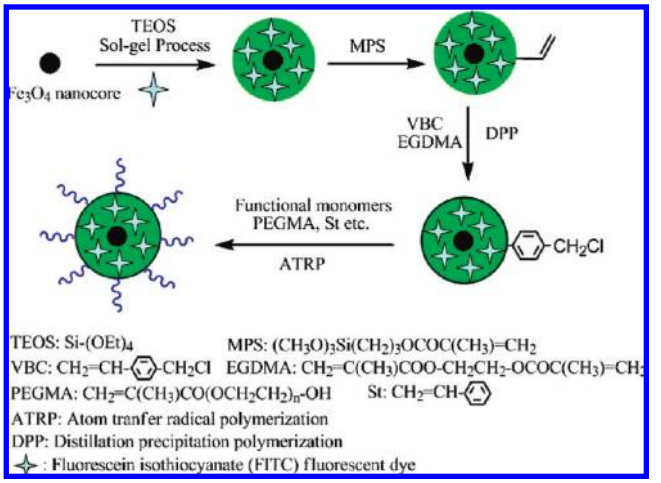

The magnetic nanoparticles have an average diameter of around 8 nm. The as-synthesized Fe_3O_4 nanoparticles tend to aggregate (Supporting Information, Figure S1). After the sol−gel reaction, the average diameter of the $Fe_3O_4/DySiO_2$ core−shell nanoparticles increases to about 73 nm. Thus, the thickness of the silica shell is about 32 nm. The TEM image of the $Fe_3O_4/DySiO_2$ core−shell nanostructure is shown in Figure 1a. The AFM image in Figure 1b shows that the magnetic and fluorescent $Fe_3O_4/DySiO_2$ core−shell nanoparticles have a smooth and well-defined surface. The maximum fluorescence of the $Fe_3O_4/DySiO_2$ nanoparticles occurs at about 518 nm (Supporting Information, Figure S2), suggesting that the FITC dye has been successfully incorporated into the silica layer of the $Fe_3O_4/DySiO_2$ core−shell nanoparticles.

The carbon−carbon double bonds on the surface of $Fe_3O_4/DySiO_2$ nanoparticles, introduced by the organosilicon coupling agent, 3-(trimethoxysilyl)propyl methacrylate (MPS), play an important role in the subsequent fabrication of core−shell hybrid nanospheres.[25] The FT-IR spectrum of the MPS-modified $Fe_3O_4/DySiO_2$ ($Fe_3O_4/DySiO_2$-MPS) nanoparticles is shown in Figure 2a. The distinct absorption band at 1637 cm^{-1} is associated with the vinyl group of MPS. The carbon−carbon double bonds on the surfaces of silica serve as polymerization sites during the subsequent distillation−precipitation polymerization. The $Fe_3O_4/DySiO_2$−PVBC hybrid nanoparticles (PVBC = poly(4-vinylbenzyl chloride)) are prepared via distillation−precipitation polymerization of 4-vinylbenzyl chloride (VBC), using the $Fe_3O_4/DySiO_2$-MPS core−shell nanoparticles as seeds. The FT-IR spectrum of the $Fe_3O_4/DySiO_2$-PVBC nanoparticles in Figure 2b shows strong absorption peaks at 710 and 1452

Published on Web 09/18/2009

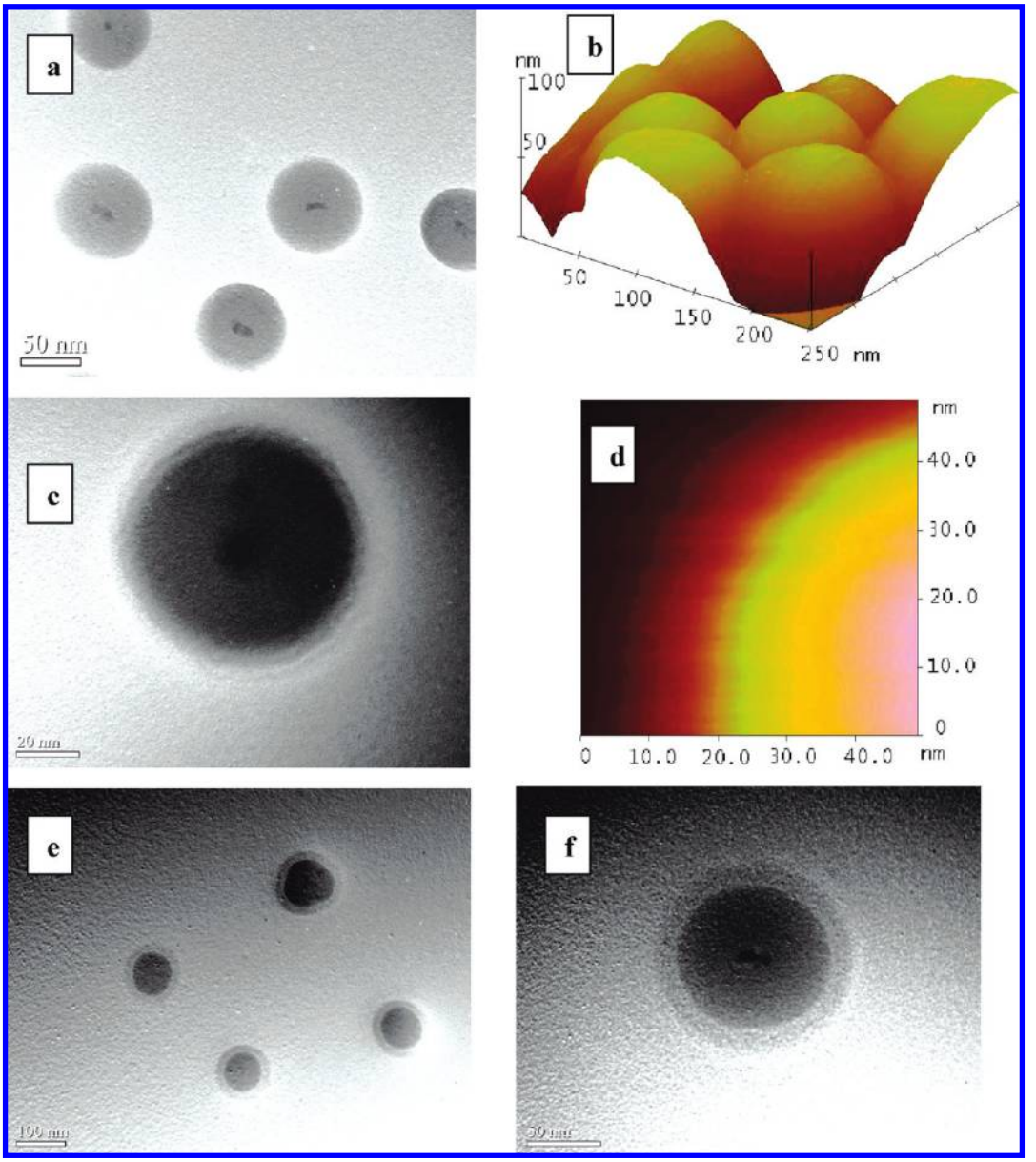

Figure 1. TEM and AFM micrographs of the (a, b) $Fe_3O_4/DySiO_2$ nanoparticles, (c, d) $Fe_3O_4/DySiO_2$-*g*-P(PEGMA) nanoparticles, and (e, f) $Fe_3O_4/DySiO_2$−PMAA nanoparticles.

cm^{-1}, associated with the vibration of phenyl group in PVBC. The X-ray photoelectron spectroscopy (XPS) wide-scan spectra of the nanoparticles before and after coating of PVBC are shown in parts a and b of Figure 3, respectively. The photoelectron lines at the binding energy (BE) of about 200 eV is associated with the covalent Cl species of the PVBC layer. The C 1s core-level spectrum of the $Fe_3O_4/DySiO_2$-PVBC nanoparticles (Figure 3c) can be curve-fitted with three peak components having BE at about 284.6, 286.3, and 288.7 eV, attributable to the C−C/C−H, C−Cl, and C═O−O species,[23] respectively. The Cl 2p core-level spectrum (Figure 3d) of the nanoparticles consists of a spin−orbit split (Cl $2p_{3/2}$ and Cl $2p_{1/2}$) doublet at the BE of 200.0 and 201.6 eV, respectively.[26]

The chloromethyl groups on the $Fe_3O_4/DySiO_2$-PVBC nanoparticle surfaces can serve as initiation sites for the subsequent surface-initiated ATRP to introduce functional polymer brushes. Poly(ethylene glycol) monomethacrylate (PEGMA), a hydrophilic and nontoxic macromonomer, is selected to modify the nanoparticle surface. The FT-IR spectrum of $Fe_3O_4/DySiO_2$-*g*-P(PEGMA) hybrid nanoparticles, with the surface-grafted

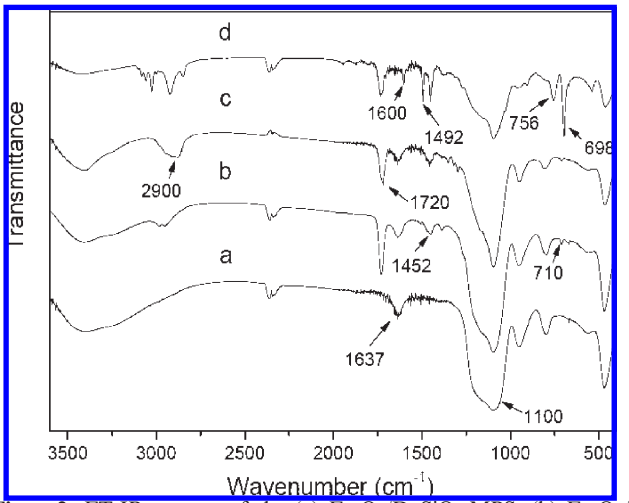

Figure 2. FT-IR spectra of the (a) $Fe_3O_4/DySiO_2$-MPS, (b) $Fe_3O_4/DySiO_2$-PVBC, (c) $Fe_3O_4/DySiO_2$-*g*-P(PEGMA), and (d) $Fe_3O_4/DySiO_2$-*g*-PS nanoparticles.

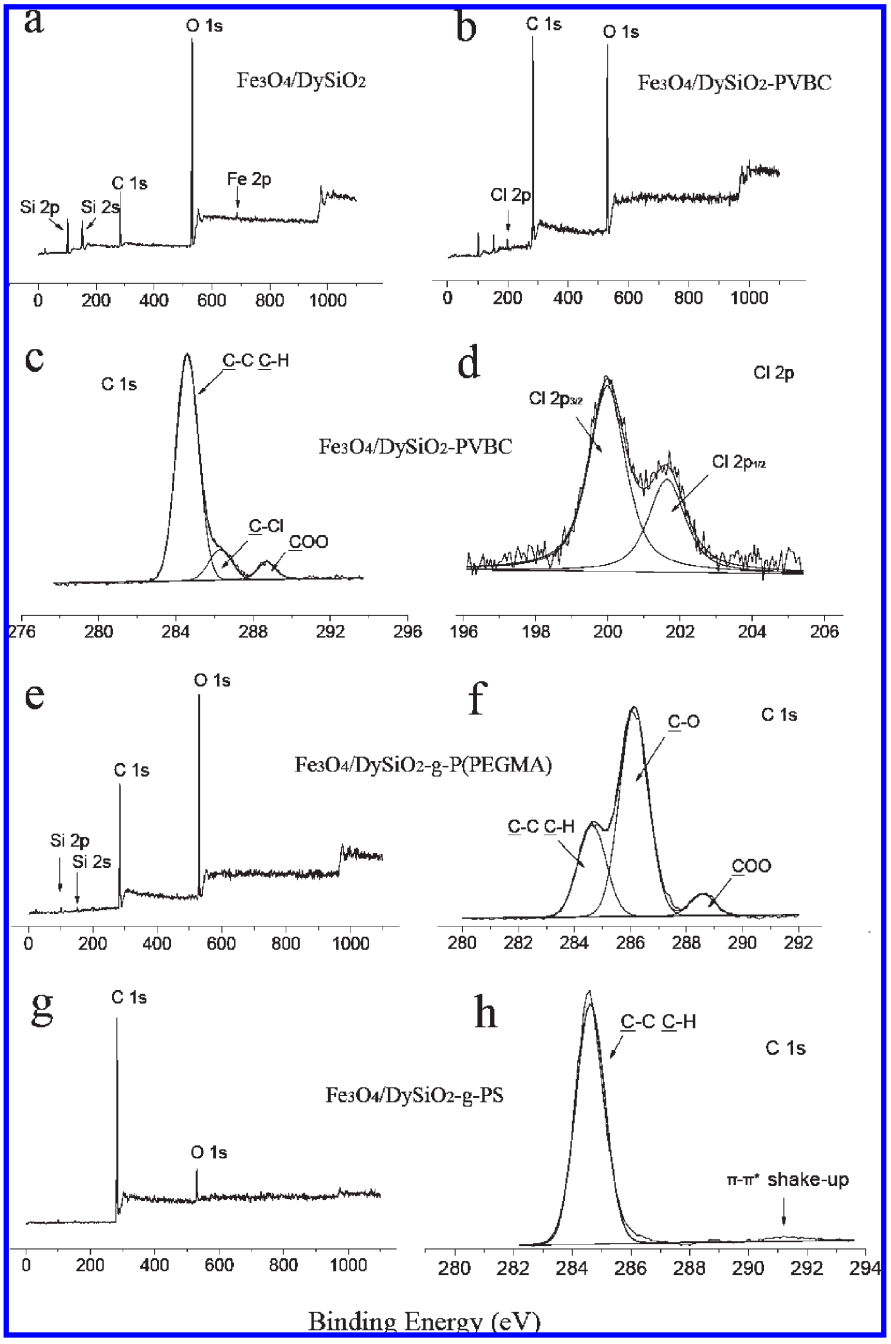

Figure 3. XPS wide-scan spectra of (a) the $Fe_3O_4/DySiO_2$ nanoparticles and (b) the $Fe_3O_4/DySiO_2$-PVBC nanoparticles; (c) C 1s and (d) Cl 2p core-level spectra of the $Fe_3O_4/DySiO_2$-PVBC nanoparticles; wide-scan and C 1s core-level spectra of (e, f) the $Fe_3O_4/DySiO_2$-*g*-P(PEGMA) nanoparticles and (g, h) the $Fe_3O_4/DySiO_2$-*g*-PS nanoparticles.

hydrophilic and biocompatible PEGMA brushes via ATRP, is shown in Figure 2c. The absorption peak at 1720 cm^{-1} is assigned to the C═O stretching vibration. The spectrum also shows a strong absorption band at around 2900 cm^{-1}, associated with the stretching vibration of $-CH_2$ groups of the P(PEGMA) brushes. The ATRP-mediated grafting of P(PEGMA) brushes on the silica shell has caused a significant decrease in the intensity of the Si signal in the XPS wide-scan spectrum of the nanospheres (Figure 3e). The C 1s core-level spectrum (Figure 3f) can be curve-fitted into three peak components with BEs at about 284.6, 286.1, and 288.6 eV, attributable to the C−C/C−H, C−O, and C═O−O species of the P(PEGMA) brushes grafted on the nanoparticle surface. The morphology of $Fe_3O_4/DySiO_2$-*g*-P(PEGMA) hybrid nanoparticles is revealed by TEM and AFM images of parts c and d of Figure 1, respectively. From the TEM image, the trilayer structure consisting of a magnetic Fe_3O_4 core, a silica inner shell, and a polymer outer shell of lower contrast is discernible. The grafted P(PEGMA) brushes are well-defined and give rise to the particles with a "hairy" surface, as suggested by the AFM image in Figure 1d. After grafting of P(PEGMA) brushes on the surface of nanoparticles, the fluorescence spectrum and the maximum emission peak (~518 nm) of the $Fe_3O_4/DySiO_2$-*g*-P(PEGMA) hybrid nanoparticles remain similar to those of the starting $Fe_3O_4/DySiO_2$ nanoparticles (Supporting Information, Figure S2). The magnetic properties of the Fe_3O_4, $Fe_3O_4/DySiO_2$, and $Fe_3O_4/DySiO_2$-*g*-P(PEGMA) nanoparticles are shown in the Supporting Information (Figure S3). The magnetic functionality is preserved in the hybrid

composites. The decrease in saturation magnetization (M_s) values in the $Fe_3O_4/DySiO_2$ and $Fe_3O_4/DySiO_2$-*g*-P(PEGMA) nanoparticles is consistent with the substantial decrease in effective mass of the magnetic cores[26] in the silica-coated and the hybrid nanoparticles.

The length of grafted polymer brushes on the particle surfaces can be easily controlled by adjusting the polymerization time.[21,27] The uptake of $Fe_3O_4/DySiO_2$-*g*-P(PEGMA) hybrid nanoparticles by cells was investigated by confocal laser scanning microscopy (CLSM). The improved biocompatibility of the $Fe_3O_4/DySiO_2$-*g*-P(PEGMA) nanoparticles, in comparison to their $Fe_3O_4/DySiO_2$ precursors, was illustrated by the increased uptake of the nanoparticles by the 3T3 fibroblasts (Supporting Information, Figure S4). The PEGMA brushes can also render the surface of nanoparticles nonfouling in delivery and diagnosis applications.[28−31]

The $Fe_3O_4/DySiO_2$-PVBC nanoparticles provide a common platform for grafting, via surface-initiated ATRP, of various functional polymer brushes on the magnetic and fluorescent nanoparticles. Styrene (St), for example, can be graft polymerized from the surface of nanoparticles to produce the hydrophobic polystyrene (PS) brushes for dispersing in organic solvents. Figure 2d shows the FT-IR spectrum of the resulting $Fe_3O_4/DySiO_2$-*g*-PS nanoparticles. The characteristic absorption bands at 1200−1600, 698, and 756 cm^{-1} are associated with the stretching vibration of the benzene ring of PS. After grafting of the PS brushes, the XPS wide-scan spectrum of the $Fe_3O_4/DySiO_2$-*g*-PS nanoparticles is dominated by the C 1s signal at the BE of about 285 eV (Figure 3g). The appearance of a high BE tail at about 291.2 eV in the C 1s core-level spectrum (Figure 3h), associated with the $\pi-\pi^*$ shake-up satellite of aromatic rings, is consistent with the presence of surface grafted PS chains. In addition, temperature and pH dual-responsive poly(2-(dimethylamino)ethyl methacrylate) (PDMAEMA)[32] can be grafted from the surface of magnetic and fluorescent core−shell nanoparticles. PDMAEMA is of importance in gene delivery systems and for protein separation, arising from its unique electrostatic interaction with DNA, enzymes, and certain drugs.[33,34]

Moreover, the degree of interaction of the encapsulated core with its surrounding environment can be controlled via adjusting the thickness and introduction of stimuli-responsive properties into the polymer shell. During distillation−precipitation polymerization, pH-responsive monomer of methacrylic acid (MAA)[25] was used instead of 4-vinylbenzyl chloride. The TEM image of the so-obtained Fe_3O_4/SiO_2-PMAA hybrid nanoparticles (Figure 1e) reveals a soft polymer shell of low contrast encapsulating a dense inorganic core. The polymer outer shell of about 15 nm in thickness is readily discernible in the TEM image of higher magnification (Figure 1f). The thickness of the PMAA shell encapsulating the inorganic core can also be regulated through response to changes in pH of the medium.

3. Conclusions

Hairy hybrid nanoparticles, consisting of a magnetic core, a fluorescent silica shell, and functional polymer brushes, have been synthesized via combined inorganic sol−gel reaction and polymer synthesis. The combined polymerization techniques of DPP and ATRP have provided a versatile tool for surface functionalization of inorganic nanoparticles and substrates. Well-defined hairy polymer brushes of hydrophilic P(PEGMA) and hydrophobic PS can be grafted from the $Fe_3O_4/DySiO_2$ core−shell nanoparticles. The interdisciplinary approach of combining inorganic and polymer syntheses, as well as DPP and ATRP techniques in the polymer syntheses, has allowed the design and synthesis of nanoparticles of sophisticated structure and function for biomaterials and biomedical applications.

4. Experimental Section

4.1. Materials. Tetraethyl orthosilicate (TEOS, 98%), 3-methacryloxypropyltrimethoxysilane (MPS, 98%), 3-aminopropyltriethoxysilane (APS, 97%), fluorescein isothiocyanate (FITC, Fluka), methacrylic acid (MAA, 99%), 4-vinylbenzyl chloride (VBC, 97%) 2,2′-bipyridyl (Bpy), ethylene glycol dimethacrylate (EGDMA, 98%), and poly(ethylene glycol) methacrylate (PEGMA, M_n 360) macromonomer were obtained from Aldrich Chemical Co. MAA was purified by vacuum distillation. PEGMA was passed through a silica gel column to remove the inhibitor, prior to being stored under an argon atmosphere at −10 °C. HPLC grade acetonitrile and analytical grade ethanol were used in all syntheses.

4.2. Synthesis of Magnetic and Fluorescent Core−Shell Nanoparticles. The fluorescent silica shell on the magnetic (Fe_3O_4) core was prepared via a modified Stöber method described below.[35] $FeCl_2 \cdot 4H_2O$ (3.135 g, 0.0157 mol) and $FeCl_3$ (5.116 g, 0.0315 mol) were added into 100 mL of deionized water. After adding 12.7 mL of NaOH (10 M), the reaction mixture was stirred for 1 h at room temperature. The reaction mixture was then heated to 90 °C under continuous stirring for another 1 h. About 0.33 mL of nitric acid was subsequently added to the reaction mixture for 0.5 h at 90 °C. Trisodium citrate (0.3 M, 50 mL) was then added, and the mixture was stirred for another 0.5 h. The reaction mixture was allowed to cool, and acetone was added to precipitate the iron oxides from the aqueous solutions. The mixture was centrifuged to collect the synthesized Fe_3O_4 nanoparticles. Deionized water was subsequently used to redisperse the Fe_3O_4 nanoparticles, and the resultant Fe_3O_4 nanoparticles were purified by dialysis for 1 week. Prior to the fabrication of $Fe_3O_4/DySiO_2$ core−shell nanoparticles, the dye solution was first prepared. About 1 mg of fluorescein isothiocyanate (FITC), 25 μL of APS, and 5 mL of ethanol were added into a test tube, and the mixture was stirred for 48 h in a vortex shaker. The $Fe_3O_4/DySiO_2$ core−shell nanoparticles were prepared using a sol−gel process. About 12 mg of Fe_3O_4 was introduced into a 250 mL round-bottom flask. Deioned water (25 mL), ethanol (120 mL), and TEOS (2 mL) were then added. The reaction mixture was sonicated for 15 min. Then, ammonia hydroxide (25 wt %, 3.8 mL) was added slowly into the reaction system with vigorous stirring. The dye solution prepared was introduced to the reaction system after 6 h. The reaction was allowed to proceed for another 18 h to form the $Fe_3O_4/DySiO_2$ core−shell nanoparticles. The core−shell nanoparticles were further modified with 3-(trimethoxysilyl)propyl methacrylate (MPS) by adding 2 mL of MPS into the reaction system, followed by stirring for 24 h. The nanoparticles were washed three times with a 1:1 (v/v) mixture of ethanol and water.

4.3. Coating of Poly(vinylbenzyl chloride) (PVBC) on $Fe_3O_4/DySiO_2$ Core−Shell Nanoparticles via Distillation−Precipitation Polymerization. The core−shell nanoparticles with surface-immobilized MPS ($Fe_3O_4/DySiO_2$-MPS, 0.1 g) were dispersed into 40 mL of acetonitrile, and the mixture was sonicated for 15 min. VBC (0.2 mL, monomer), EGDMA (0.3 mL, cross-linking agent), and AIBN (10 mg, initiator) were subsequently added to the system. The round-bottom flask was fitted with a fractionation column, a Liebig condenser, and a receiver. The reaction mixture was brought to boiling and was maintained under reflux condition. The reaction was stopped after ~10 mL of the acetonitrile had been distilled off from the reaction system in about 2 h. The resulting $Fe_3O_4/DySiO_2$-PVBC nanoparticles were collected by centrifugation, washed with ethanol, and dried in a vacuum oven at 50 °C. For the preparation of $Fe_3O_4/DySiO_2$-PMAA hybrid nanoparticles, about 0.2 mL of the methacrylic acid (MAA), instead of VBC, was introduced into the reaction system before starting the polymerization reaction.

4.4. Graft Polymerization of Poly((ethylene glycol) monomethacrylate) (PEGMA) and Styrene (St) from the $Fe_3O_4/DySiO_2$-PVBC Nanopartilces via Surface-Initiated Atom Transfer Radical Polymerization (ATRP). Surface-initiated ATRP was carried out to produce the $Fe_3O_4/DySiO_2$-*g*-P(PEGMA)

hybrid nanoparticles. About 50 mg of Fe_3O_4/$DySiO_2$-PVBC nanoparticles was introduced into a pyrex tube. About 5 mL of PEGMA was added to disperse the dried nanoparticles. The catalyst (CuCl, 4.3 mg) and ligand (Bpy, 20 mg) were then added. The mixture was degassed with purified argon for 15 min. The pyrex tube was sealed, and the reaction mixture was stirred in a 30 °C water bath for 24 h. After the reaction had completed, the reaction mixture was diluted with THF (25 mL, 1:5 ratio), and the nanoparticles were precipitated in diethyl ether. The Fe_3O_4/$DySiO_2$-*g*-P(PEGMA) hybrid nanoparticles were washed with ethanol, centrifuged, and dried. The polystyrene brushes were grafted from the Fe_3O_4/$DySiO_2$-PVBC nanoparticles via the similar surface-initiated ATRP process, except the polymerization temperature was raised to 120 °C.

4.5. Characterization. Transmission electron microscopy (TEM) images were obtained on a JEOL JEM-2010 TEM. The morphology of the resulting nanoparticles was studied by atomic force microscopy (AFM), using a Nanoscope IIIa AFM system. Fourier transform infrared (FT-IR) spectroscopy analysis was carried out on a Bio-Rad FTS-135 spectrophotometer. Fluorescence emission spectra were measured on a Shimadzu RF-5301PC spectrofluorophotometer with light of 450 nm as excitation source. The samples were prepared from suspension of the nanoparticles in ethanol with concentration of about 5 mg/mL. X-ray photoelectron spectroscopy (XPS) measurements were carried out on a Kratos AXIS HSi spectrometer equipped with a monochromatized Al Kα X-ray source (1468.6 eV photons). Confocal laser scanning microscopy (CLSM) images were obtained on a Nikon Digital Eclipse C1 Plus confocal system. A vibrating-sample magnetometer (VSM; model 7304, Lakeshore, Westerville, OH) were used to measure the magnetic moment at room temperature.

Supporting Information Available: TEM image of the Fe_3O_4 nanoparticles, fluorescence emission spectrum of the Fe_3O_4/$DySiO_2$ and Fe_3O_4/$DySiO_2$-*g*-P(PEGMA) hybrid nanoparticles, magnetic measurements of the nanoparticles, and CLSM images of the uptake of Fe_3O_4/$DySiO_2$-*g*-P(PEGMA) nanoparticles by 3T3 fibroblasts. This material is available free of charge via the Internet at http://pubs.acs.org.

References and Notes

(1) Selvan, S. T.; Patra, P. K.; Ang, C. Y.; Ying, J. Y. *Angew. Chem., Int. Ed.* **2007**, *46*, 2448–2452.
(2) Deng, Y.; Qi, D.; Deng, C.; Zhang, X.; Zhao, D. *J. Am. Chem. Soc.* **2008**, *130*, 28–29.
(3) Guo, J.; Yang, W.; Deng, Y.; Wang, C.; Fu, S. *Small* **2005**, *1*, 737–743.
(4) Wuang, S. C.; Neoh, K. G.; Kang, E. T.; Pack, D. W.; Leckband, D. E. *Biomaterials* **2008**, *29*, 2270–2279.
(5) Gupta, A. K.; Gupta, M. *Biomaterials* **2005**, *26*, 3995–4021.
(6) Yoon, T.; Kim, J. S.; Kim, B. G.; Yu, K. N.; Cho, M. H.; Lee, J. K. *Angew. Chem., Int. Ed.* **2005**, *44*, 1068–1071.
(7) Salgueiriño-Maceira, V.; Correa-Duarte, M. A.; Sapsova, M.; Liz-Marzán, L. M.; Farle, M. *Adv. Funct. Mater.* **2006**, *16*, 509–514.
(8) Nagao, D.; Yokoyama, M.; Yamauchi, N.; Matsumoto, H.; Kobayashi, Y.; Konno, M. *Langmuir* **2008**, *24*, 9804–9808.
(9) Kamata, K.; Lu, Y.; Xia, Y. *J. Am. Chem. Soc.* **2003**, *125*, 2384–2385.
(10) Li, G. L.; Kang, E. T.; Neoh, K. G.; Yang, X. *Langmuir* **2009**, *25*, 4361–4364.
(11) Fulghum, T. M.; Estillore, N. C.; Vo, C. D.; Armes, S. P.; Advincula, R. C. *Macromolecules* **2008**, *41*, 429–435.
(12) Lee, H.; Jakubowski, W.; Matyjaszewski, K.; Yu, S.; Sheiko, S. *Macromolecules* **2006**, *39*, 4983–4989.
(13) Quémener, D.; Davis, T. P.; Barner-Kowollik, C.; Stenzel, M. H. *Chem. Commun.* **2006**, 5052–5053.
(14) Zhang, X.; Lian, X.; Liu, L.; Zhang, J.; Zhao, H. *Macromolecules* **2008**, *41*, 7863–7869.
(15) Li, M.; De, P.; Gondi, S. R.; Sumerlin, B. S. *Macromol. Rapid Commun.* **2008**, *29*, 1172–1176.
(16) Ober, C. K.; Cheng, S. Z. D.; Hammond, P. T.; Muthukumar, M.; Reichmanis, E.; Wooley, K. L.; Lodge, T. P. *Macromolecules* **2009**, *42*, 465–471.
(17) Bai, F.; Yang, X. L.; Huang, W. Q. *Macromolecules* **2004**, *37*, 9746–9752.
(18) Li, G. L.; Yang, X. L. *J. Phys. Chem. B* **2007**, *111*, 12781–12786.
(19) Li, G. L.; Lei, C.; Wang, C.; Neoh, K. G.; Kang, E. T.; Yang, X. *Macromolecules* **2008**, *41*, 9487–9490.
(20) Matyjaszewski, K.; Tsarevsky, N. V. *Nat. Chem.* **2009**, *1*, 176–288.
(21) Pyun, J.; Kowalewski, T.; Matyjaszewski, K. *Macromol. Rapid Commun.* **2003**, *24*, 1043–1059.
(22) Couet, J.; Biesalski, M. *Macromolecules* **2006**, *39*, 7258–7268.
(23) Xu, F. J.; Kang, E. T.; Neoh, K. G. *Macromolecules* **2005**, *38*, 1573–1580.
(24) Fu, G. D.; Zhao, J. P.; Sun, M.; Kang, E. T.; Neoh, K. G. *Macromolecules* **2007**, *40*, 2271–2275.
(25) Li, G. L.; Liu, G.; Kang, E. T.; Neoh, K. G.; Yang, X. *Langmuir* **2008**, *24*, 9050–9055.
(26) Fan, Q. L.; Neoh, K. G.; Kang, E. T.; Shuter, B.; Wang, S. C. *Biomaterials* **2007**, *28*, 5426–5436.
(27) Fu, G. D.; Shang, Z. H.; Hong, L.; Kang, E. T.; Neoh, K. G. *Macromolecules* **2005**, *38*, 7867–7871.
(28) Waku, T.; Matsusaki, M.; Kaneko, T.; Akashi, M. *Macromolecules* **2007**, *40*, 6385–6392.
(29) Zhang, Y.; Kohler, N.; Zhang, M. *Biomaterials* **2002**, *23*, 1553–1561.
(30) Cu, Y.; Saltzman, W. M. *Mol. Pharmaceutics* **2009**, *6*, 173–181.
(31) Salgueiriño-Maceira, V.; Correa-Duarte, M. A. *Adv. Mater.* **2007**, *19*, 4131–4144.
(32) Xue, J.; Chen, L.; Wang, H. L.; Zhang, Z. B.; Zhu, X. L.; Kang, E. T.; Neoh, K. G. *Langmuir* **2008**, *24*, 14151–14158.
(33) Zhang, G.; Stöver, H. D. H. *Macromolecules* **2003**, *36*, 7439–7445.
(34) Lee, S. B.; Koepsel, R. R.; Morley, S. W.; Matyjaszewski, K.; Sun, Y.; Russell, A. J. *Biomacromolecules* **2004**, *5*, 877–882.
(35) Lu, Y.; Yin, Y.; Mayers, B. T.; Xia, Y. *Nano Lett.* **2002**, *2*, 183–186.